

# Ada3D : Exploiting the Spatial Redundancy with Adaptive Inference for Efficient 3D Object Detection

Tianchen Zhao<sup>12</sup>, Xuefei Ning<sup>1\*</sup>, Ke Hong<sup>1</sup>, Zhongyuan Qiu<sup>2</sup>, Pu Lu<sup>1</sup>, Yali Zhao<sup>2</sup>,  
Linfeng Zhang<sup>1</sup>, Lipu Zhou<sup>3</sup>, Guohao Dai<sup>4</sup>, Huazhong Yang<sup>1</sup>, Yu Wang<sup>1\*</sup>

<sup>1</sup>Tsinghua University, <sup>2</sup>Novauto, <sup>3</sup>Meituan, <sup>4</sup>Shanghai Jiao Tong University

{suozhang1998, foxdoraame}@gmail.com {zhongyuan.qiu, yali.zhao}@novauto.com.cn

{zhanglinfeng1997, zhoulipu}@outlook.com daiguohao@sjtu.edu.cn

{hongk21, lup22, yanghz, yu-wang}@mail.tsinghua.edu.cn

## Abstract

Voxel-based methods have achieved state-of-the-art performance for 3D object detection in autonomous driving. However, their significant computational and memory costs pose a challenge for their application to resource-constrained vehicles. One reason for this high resource consumption is the presence of a large number of redundant background points in Lidar point clouds, resulting in spatial redundancy in both 3D voxel and BEV map representations. To address this issue, we propose an adaptive inference framework called **Ada3D**, which focuses on reducing the **spatial redundancy** to compress the model's computational and memory cost. Ada3D adaptively filters the redundant input, guided by a lightweight importance predictor and the unique properties of the Lidar point cloud. Additionally, we maintain the BEV features' intrinsic sparsity by introducing the Sparsity Preserving Batch Normalization. With Ada3D, we achieve 40% reduction for 3D voxels and decrease the density of 2D BEV feature maps from 100% to 20% without sacrificing accuracy. Ada3D reduces the model computational and memory cost by 5 $\times$ , and achieves 1.52 $\times$  / 1.45 $\times$  end-to-end GPU latency and 1.5 $\times$  / 4.5 $\times$  GPU peak memory optimization for the 3D and 2D backbone respectively.

## 1. Introduction

The perception of the 3D scene plays a vital role in autonomous driving systems. It's essential that the perception of the surrounding 3D scene is both quick and accurate, which places high demands on both performance and latency for perception methods.

Voxel-based 3D deep learning methods convert the in-

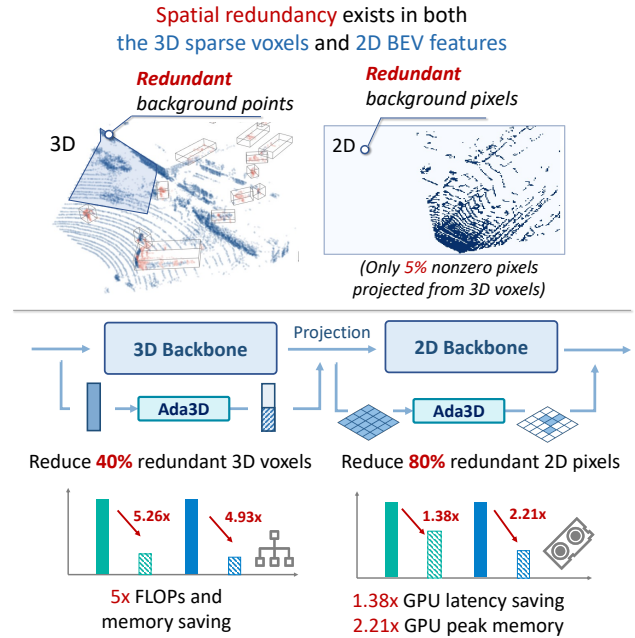


Figure 1: Ada3D is an adaptive inference framework that exploits the spatial redundancy for both the 3D voxel and 2D BEV features.

put point cloud into sparse voxels by quantizing them into regular grids, and achieve state-of-the-art performance [9]. However, current voxel-based methods struggle to meet the real-time demand on self-driving cars due to constrained resources [10]. As a result, it is crucial to improve the efficiency of voxel-based 3D perception methods (e.g., reduce the GPU latency and peak memory).

There are two main factors contributing to the excessively long processing time for 3D perception methods. Firstly, the model size is excessive, and it contains time-consuming operations such as 3D sparse convolution [10].

\*Corresponding Authors

Secondly, the algorithm needs to process a large amount of input points (e.g., 30K for nuScenes). Prior researches focus on solving the former issue by compressing the model both at the operation-level [5, 11] and architecture-level [20, 26]. In this paper, we take a different approach and improve the model’s efficiency from the data level.

The typical pipeline of voxel-based 3D detector is displayed in Fig. 1, the 3D backbone extracts feature from the input point cloud. The 3D features are then projected to bird-eye-view (BEV) space along the z-axis and further processed by the 2D backbone with normal 2D convolutions.

We discover that there exists spatial redundancy for both the 3D voxel and 2D BEV features. For 3D voxels, As shown in Fig. 1, a large number of points in the input point cloud represents the road plane and buildings, which are redundant “background” for 3D detection. We further validate the redundancy of the point cloud with quantitative results in Fig. 2. When we randomly drop 30% of the input points or 70% of the points excluding those within the ground-truth bounding box (the “foreground”), we only observe a subtle drop in performance. Existing 3D CNNs treat all input points equally, thus wasting a substantial amount of computation and memory on the less-informative background area. Regarding 2D BEV features, as shown in Fig. 1, only a small portion of (e.g., 5% for KITTI) pixels have projected feature values in the BEV space, while others are background pixels with zero value. However, current methods treat these sparse BEV features as dense and apply normal CNN to them. As can be observed in the lower part of Fig. 2, the feature map loses sparsity after the first batch normalization layer, which fails to utilize the sparse nature of the Lidar-projected BEV feature map.

To compress the data’s spatial redundancy, we propose an adaptive inference method **Ada3D**. We adopt adaptive inference to both the 3D and 2D backbone and selectively filter out redundant 3D voxels and 2D BEV features during inference. We employ a lightweight predictor to evaluate the importance of input features in the BEV space. The predictor score is combined with the density of the Lidar point cloud to determine which features to drop. In addition, we introduce a simple yet effective technique called sparsity-preserving batch normalization, which efficiently eliminates background pixels and preserves sparsity for 2D BEV features. Through adaptively skipping redundant features, Ada3D reduces the computational and memory costs of the model by  $5\times$  and achieves  $1.4\times$  end-to-end speedup and  $2.2\times$  GPU peak memory optimization on RTX3090 without compromising performance.

The contributions of this paper could be summarized into three aspects, as follows:

1. We introduce the adaptive inference method Ada3D that leverages spatial redundancy for efficient 3D object detection.

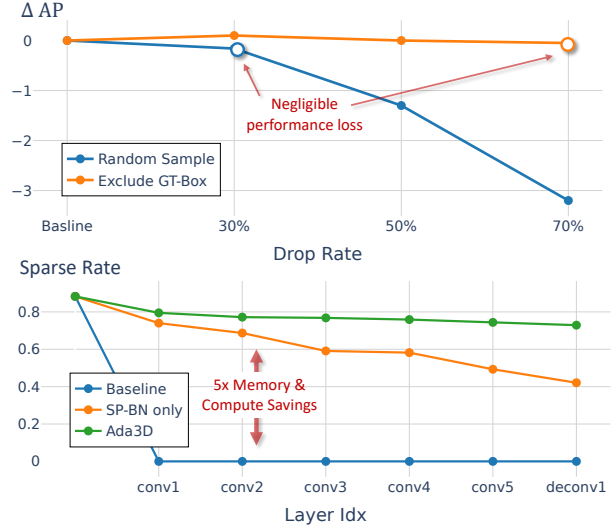


Figure 2: **Empirical evidence of spatial redundancy in 3D and 2D data.** Upper: The KITTI Cars Moderate AP under different drop rates with random dropping and ground-truth excluded dropping. Lower: The sparsity of different layer’s 2D BEV features.

2. We design a shared predictor to evaluate the importance of input features, and combine the predictor score with point cloud density as the criterion for dropping redundant features.
3. We propose sparsity-preserving batch normalization to maintain the sparsity for the 2D backbone.

## 2. Related Works

### 2.1. Voxel-based 3D Detection Methods

Voxel-based methods convert the point cloud into regular grids. SECOND [21] utilizes the 3D sparse convolution for feature extraction. CenterPoint [25] is a single-stage detector that leverages a keypoint detector to detect box centers. PV-RCNN [15] combines the point and voxel features and utilizes a two-staged framework for precise detection. While the voxel-based detectors achieve state-of-the-art results, their high computational and memory costs impede their application on self-driving cars. Ada3D aims to alleviate this issue through adaptive inference.

### 2.2. Adaptive inference for 2D image

In the field of 2D perception, adaptive inference methods reduce spatial redundancy for 2D images. Figurnov *et. al.* [1] dynamically adjust depth for different regions. Channel gating network [6] and SBNet [14] learn to adaptively skip redundant channel/pixels. GFNet [7] employs reinforcement learning to locate the discriminant regions.

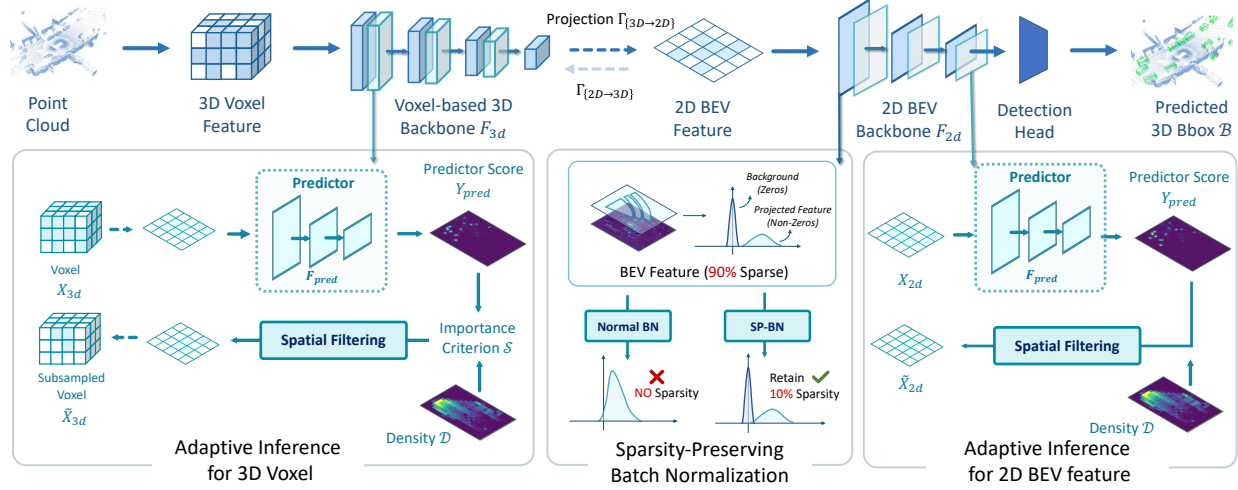


Figure 3: **The overall framework of Ada3D.** Adaptive inference is conducted in both the 3D and 2D backbone. The spatial filtering module combines the predictor score and 3D point cloud’s density to drop the redundant parts. Furthermore, the SP-BN is introduced to omit the background pixels in 2D backbone and retain sparsity.

Ada3D applies adaptive inference to the 3D perception, and adaptively filters redundant 3D voxels and BEV features.

### 2.3. Efficient 3D Detection Methods

Some prior studies aim to enhance the efficiency of 3D detectors. SPVNAS [20] employs neural architecture search to search for suitable depth and width for the 3D model. Lee *et. al.* [5] propose a point-distribution pruning method on 3D convolution kernel. SPS-Conv [11] prunes the output mapping for sparse convolution based on the feature magnitude. IASSD [28] and DB-SSD [22] design novel feature-based downsampling to replace time-consuming furthest point sampling (FPS) for point-based 3D detectors. These methods optimize the efficiency of 3D detectors from the perspective of compressing model redundancy. Differently, Ada3D focuses on reducing spatial redundancy and could work on par with these methods.

## 3. Methods

### 3.1. Voxel-based Detection with Adaptive Inference

Figure 3 illustrates the overall framework of Ada3D. The 3D object detection task aims to predict 3D bounding boxes  $\mathcal{B} = \{b_k\}$  from the point cloud  $\mathcal{P} = \{(x, y, z, r)_i\}$ . The voxel-based 3D detectors [15, 21, 25] quantize the point cloud into regular grids. Without loss of generality, we omit the batch dimension in the following equations. The voxelization generates sparse voxels  $\mathbf{X}_{3d} \in \mathbb{R}^{N \times C}$  of voxel numbers  $N$  and feature channels  $C$ . The 3D voxel backbone  $\mathbf{F}_{3d}$  applies 3D sparse convolution [2] on the voxels to extract point cloud feature. We use the  $\mathbf{X}_{i,c}$  to represent the  $c$ -th channel of  $i$ -th voxel feature, and the  $c'$  channel of

the  $j$ -th output voxel can be described as:

$$\mathbf{Y}_{j,c'} = \sum_k \sum_c W_{k,c,c'} X_{R_{k,j},k,c}, \quad (1)$$

where  $R_{k,j}$  is the input index  $i$  given the output index  $j$  and kernel offset  $k$ ,  $W_{k,c,c'}$  denotes the kernel offset  $k$ ’s weight.

The processed 3D feature  $\tilde{\mathbf{X}}_{3D}$  is then projected to the BEV plane through sum pooling along the  $z$ -axis to generate 2D features  $\mathbf{X}_{2D} \in \mathbb{R}^{C \times W \times H}$ . We define  $\Gamma_{3D \rightarrow 2D}$  as the mapping from 3D voxels to 2D BEV pixels, and  $\Gamma_{2D \rightarrow 3D}$  describes the invert mapping. The 2D BEV backbone  $\mathbf{F}_{2D}$  is applied to further extract the 2D BEV feature. Finally, the detection head  $\mathbf{F}_{head}$  predicts the 3D bounding box.

The adaptive inference is adopted in both the 3D and 2D backbone. For simplicity, we omit the channel dimension  $C$  for feature  $\mathbf{X}$  for the equations below, since all channels share the same spatial filtering pattern. We describe the layer indexes where the predictor is applied with the layer index  $\mathcal{I}_{3D} = \{l_{3D}^{(1)}, \dots, l_{3D}^{(n)}\}$  and  $\mathcal{I}_{2D} = \{l_{2D}^{(1)}, \dots, l_{2D}^{(n)}\}$ .

The adaptive inference for 3D backbone could be described as:

$$\begin{aligned} \text{for } l_{3D}^{(i)} \in \mathcal{I}_{3D} : \mathbf{X}_{3D}^{(l_{3D}^{(i)})} &= \mathbf{F}_{3D}^{(l_{3D}^{(i)})}(\tilde{\mathbf{X}}_{3D}^{(l_{3D}^{(i)}-1)}), \text{ where} \\ \tilde{\mathbf{X}}_{3D}^{(l_{3D}^{(i)}-1)} &= \Gamma_{2D \rightarrow 3D}(\mathbf{F}_{drop}(\Gamma_{3D \rightarrow 2D}(\mathbf{X}_{3D}^{(l_{3D}^{(i)}-1)}), \mathbf{S})) \odot \mathbf{X}_{3D}^{(l_{3D}^{(i)}-1)}, \\ \mathbf{S} &= \mathbf{F}_{score}(\Gamma_{3D \rightarrow 2D}(\mathbf{X}_{3D}^{(l_{3D}^{(i)}-1)})), \end{aligned} \quad (2)$$

where the  $\mathbf{S} \in \mathbb{R}^{W \times H}$  represents the importance score for BEV pixels, which is generated by  $\mathbf{F}_{score}$  that combines

the predictor output and 3D point cloud’s density. The  $\mathbf{F}_{\text{score}}$  takes the 2D BEV input projected from the input 3D voxel feature  $\mathbf{X}_{3D}^{(l_{3D}^{(i)}-1)} \in \mathbb{R}^N$ . Given the drop ratio  $R_{\text{drop}}$ , the spatial filtering process  $\mathbf{F}_{\text{drop}}$  drops the most redundant portion of features in the BEV space based on the importance score  $\mathbf{S}$ . It generates the one-hot mask that indicates whether the given location should be kept or discarded. The mask is then broadcasted back to the voxel space through  $\Gamma_{2D \rightarrow 3D}$  and element-wisely multiplied with the original 3D voxel feature to generate subsampled 3D voxel feature  $\tilde{\mathbf{X}}_{3D}^{(l_{3D}^{(i)}-1)}$ . Note that the equation describes the algorithmic simulation of spatial filtering, while in the actual GPU processing, features with zero values in  $\tilde{\mathbf{X}}_{3D}^{(l_{3D}^{(i)}-1)}$  are excluded to achieve actual hardware acceleration, i.e., their computation and storage are skipped. More details about  $\mathbf{F}_{\text{drop}}$  and  $\mathbf{F}_{\text{score}}$  will be discussed in Sec. 3.2 and Sec. 3.3.

Similarly, the adaptive inference for the 2D BEV backbone is applied at  $\mathcal{I}_{2D} = \{l_{2D}^{(1)}, \dots, l_{2D}^{(n)}\}$  layers with similar process described in Equ. 2 without the transformation  $\Gamma_{2D \rightarrow 3D}, \Gamma_{3D \rightarrow 2D}$  between the voxel and the BEV space.

### 3.2. Importance Predictor Design

As discussed in Equ. 2 in Sec. 3.1, the  $\mathbf{F}_{\text{score}}$  is used for evaluating the input feature to identify its redundant parts. In Ada3D, we adopt a lightweight CNN as the spatial-wise importance predictor in BEV space to predict pixel-wise importance score from the input feature.

**Inference.** The predictor inference for 3D voxel feature is described as:

$$\mathbf{Y}_{\text{pred}} = \mathbf{F}_{\text{pred}}(\mathbf{X}_{\text{BEV}}; \Theta_{\text{pred}}), \quad (3)$$

where  $\mathbf{F}_{\text{pred}}$  is the predictor with the parameter  $\Theta_{\text{pred}}$ . The predictor’s output is a single channel heatmap  $\mathbf{Y}_{\text{pred}} \in [0, 1]^{W \times H}$ . We choose to design the predictor in the BEV space instead of 3D space, as the perception is mainly conducted in the former. Intuitively, there exists less redundancy in the vertical space, and the efficiency improvement of compressing it is restricted. Also, estimating the importance of the whole 3D space is more challenging. In order to effectively and efficiently evaluate the importance, we design a lightweight predictor that is shared for different layers at both the 3D and 2D backbone. It consists of multiple group convolutions [27] with reduced parameters and computational complexity. Besides, the resolution of the predictor is selected as 1/8 of the original original BEV resolution. The computational cost of the predictor’s is less than 1% of the 2D backbone, thereby bringing negligible overhead.

**Training.** Our oracle experiment in Fig. 2 shows that the performance only decreases slightly when dropping a notable amount of points outside the ground-truth bounding boxes. It reveals that the center of the bounding box is

of high importance and the importance spreads to the local region. Therefore, following CenterPoint [25], we generate the ground-truth heatmap  $M_{\text{gt}}$  for the predictor by rendering a 2D Gaussian circle with a peak located at each bounding box center  $(u, v)$ , which could be formulated as follows:

$$M_{\text{gt}} = \sum_{b_i} \mathcal{G}((u, v)_i, \sigma), \quad (4)$$

where  $b_i$  is the ground-truth bounding box, and  $\mathcal{G}$  is the 2D gaussian function with radius  $\sigma$ . The mean squared error (MSE) loss is adopted for predictor training.

### 3.3. Density-guided Spatial Filtering

The spatial filtering  $\mathbf{F}_{\text{drop}}$  in Equ. 2 in Sec. 3.1 describes the process of dropping the most redundant  $R_{\text{drop}}$  of the input features based on the importance criterion  $\mathbf{S}$ . We combine the predictor score with the point cloud density to determine where to drop.

The predictor score  $\mathbf{Y}_{\text{pred}}$  could effectively represent the relative importance of the input feature. However, due to the imaging principle of the Lidar sensor, the point cloud closer to the sensor has a larger density, and the remote part is sparse [29]. Due to the neighboring aggregation characteristic of the convolution, the predictor tends to output higher results for denser regions and could miss the remote objects (as shown in Fig. 9). To compensate for this bias, we propose density-guided spatial filtering that takes the unique properties of the Lidar point cloud into consideration. Specifically, we use the point cloud BEV density to adjust the predictor score. Therefore, the importance criterion  $\mathbf{S}$  is calculated as follows:

$$\mathbf{S} = \mathbf{F}_{\text{score}}(\mathbf{X}_{\text{BEV}}) = \mathbf{F}_{\text{pred}}(\mathbf{X}; \Theta_{\text{pred}}) \cdot (\mathbf{D}_g)^\beta, \quad (5)$$

where  $D$  is the density heatmap pooled with kernel size of  $g$ , and  $\beta$  is a hyperparameter that tunes the density distribution. The value of  $\beta$  is selected for each dataset with the goal of aligning the variance of the predictor score and density distribution on 10 sampled scenes. Example in Fig. 9 demonstrates that the density guidance enlarges the importance score for sparser regions and avoids mistakenly dropping the remote objects.

### 3.4. Sparsity Preserving Batch Normalization

As illustrated in Fig. 4, the 2D feature map projected from 3D voxel features in the BEV plane is sparse, only 5% and 20% features are nonzero for KITTI and nuScenes (the orange part). The rest of the background pixels (the blue ones) are initialized as zero. However, current methods do not utilize such sparsity, and the feature map loses sparsity after the first batch normalization layer (See Fig. 2). A large amount of computation and memory is wasted for the “background” features with limited information.

A straightforward way to preserve sparsity in 2D BEV backbone is to apply batch normalization only for the nonzero elements. This approach is described as the “Nonzero BN” in Fig. 4. However, we empirically discover that replacing the “Normal BN” with “Nonzero BN” causes instability in training and moderate performance degradation. We attribute this problem to the violation of the feature’s relative relations. As shown in Fig. 4, the orange part with diagonal hatching has larger values than the background features (zero), but after the “Nonzero BN”, their values are smaller than the background. To address this problem, we propose a simple but effective modification to the “Nonzero BN” and introduce the “Sparsity-preserving BN”. In order to preserve the features’ relative relations, the SP-BN leaves out the procedure of subtracting the feature’s mean. Therefore, most parts of the nonzero elements remain positive and are distinguishable from the “background”. SP-BN can be formulated as:

$$\hat{x}_i^{(k)} = \frac{x_i^{(k)}}{\sqrt{(\sigma_B^{(k)})^2 + \epsilon}}, \quad (6)$$

where  $\sigma_B^{(k)}$  is the standard deviation. Experimental results show that when replacing the normal batch normalization with SP-BN, we could increase the sparsity of 2D BEV heatmap from 0% to 50% without loss of performance.

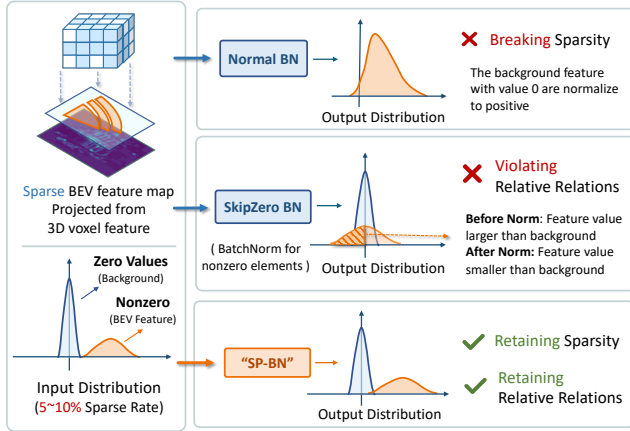


Figure 4: Comparison of our proposed sparsity preserving BN with “Normal BN” and “Nonzero BN”.

## 4. Experiments

### 4.1. Implementation Details

**KITTI and nuScenes dataset** The KITTI dataset has 7481 training images and 7518 test images with corresponding point clouds. The object to detect have 3 classes: car, pedestrian, and cyclist, the boxes are classified into three

subsets: “Easy”, “Moderate” and “Hard” based on the levels of difficulty. The detection results are evaluated by average precision (AP) for each subset with IoU threshold 0.7 for cars and 0.5 for pedestrians and cyclists. The nuScenes dataset comprises 1000 driving sequences with annotations in the form of bounding boxes for 10 object classes. The commonly used metrics are the mean Average Precision (mAP) and the nuScenes detection score (NDS). NDS is the weighted average of mAP and other box characteristics, such as translation and orientation.

**Adaptive inference design** We apply Ada3D to CenterPoint [25] model on both datasets. Due to the original CenterPoint paper does not conduct experiments on KITTI, we follow the author’s released code [23] to construct the CenterPoint model on KITTI. We replace all the batch normalization layers in the 2D backbone with sparsity-preserving BN. We apply adaptive inference at the 2nd and 4th layer of the 3D and 2D backbone. The  $R_{drop}$  is a hyperparameter (e.g., 25%/50%) to control how many features to drop. The predictor’s input resolution is set as the scene size divided by voxel size  $\times 8$ . Max poolings and same padding upsampling layers are adopted to align features of different sizes. The predictor consists of 3 convolution layers with channel size [16, 32, 16] and group size of 8. The predictor is trained with adam optimizer with one-cycle learning rate scheduling [3] of learning rate 0.003 for 10 epochs. To recover the performance, we adopt an interleaved scheme that alternates between finetuning the model with adaptive inference for 5 (2 for nuScenes) epochs and training the predictor for 1 epoch and repeat this process for a total of 5 times. The  $\sigma$  for ground-truth heatmap is 5.0. The density guidance  $\beta$  is set as 0.5 and 0.7 for KITTI and nuScenes.

**Hardware experiments settings** We measure the latency and memory usage of convolution layers on an Nvidia RTX 3090 GPU using CUDA 11.1. We implemented sparse convolution operations using the gather-GEMM-scatter dataflow in TorchSparse v2.0.0 [19] and SpConv v2.2.6 [2]. To measure latency, we synchronized the GPU and recorded the starting and ending times. To measure peak memory usage, we embedded the PyTorch Memory Utils [13] into the engine frontend.

### 4.2. Performance and Efficiency Comparison

We first present the performance and resource consumption of Ada3D optimized model on KITTI and nuScenes. We estimate the memory cost of the model by summing the intermediate activation sizes following recent literature [18]. As could be seen from Table. 1, **the Ada3D optimized model achieves comparable performance with other methods of different paradigms while compressing the model’s computational and memory cost.** In Table. 3 and Fig. 5, we present Ada3D model with different drop rates. The model size could be effectively tuned



Table 1: **Performance comparison of Ada3D and other methods on KITTI *test* set.** The “Ada3D-B” and “Ada3D-C” are centerpoint models optimized by Ada3D with different drop rates.

Mehod	<i>FLOPs</i>	<i>Mem</i>	mAP ( <i>Mod.</i> )	3D Car (IoU=0.7)			3D Ped. (IoU=0.5)			3D Cyc. (IoU=0.5)		
	<i>Opt.</i>	<i>Opt.</i>		<i>Easy</i>	<i>Mod.</i>	<i>Hard</i>	<i>Easy</i>	<i>Mod.</i>	<i>Hard</i>	<i>Easy</i>	<i>Mod.</i>	<i>Hard</i>
VoxelNet [30]	-	-	49.05	77.47	65.11	57.73	39.48	33.69	31.50	61.22	48.36	44.37
SECOND [21]	-	-	57.43	84.65	75.96	68.71	45.31	35.52	33.14	75.83	60.82	53.67
PointPillars [8]	-	-	58.29	82.58	74.31	68.99	51.45	41.92	38.89	77.10	58.65	51.92
SA-SSD [4]	-	-	-	88.75	79.79	74.16	-	-	-	-	-	-
TANet [12]	-	-	59.90	84.39	75.94	68.82	53.72	44.34	40.49	75.70	59.44	52.53
Part-A <sup>2</sup> [17]	-	-	61.78	87.81	78.49	73.51	53.10	43.35	40.06	79.17	63.52	56.93
SPVCNN [20]	-	-	61.16	87.80	78.40	74.80	49.20	41.40	38.40	80.10	63.70	56.20
PointRCNN [16]	-	-	57.95	86.96	75.64	70.70	47.98	39.37	36.01	74.96	58.82	52.53
3DSSD [24]	-	-	55.11	87.73	78.58	72.01	35.03	27.76	26.08	66.69	59.00	55.62
IA-SSD [28]	-	-	60.30	88.34	80.13	75.10	46.51	39.03	35.60	78.35	61.94	55.70
CenterPoint [25]	-	-	59.96	88.21	79.80	76.51	46.83	38.97	36.78	76.32	61.11	53.62
CenterPoint-Pillar [25]	-	-	57.39	84.76	77.09	72.47	44.07	37.80	35.23	75.17	57.29	50.87
CenterPoint (Ada3D-B)	<b>5.26×</b>	<b>4.93×</b>	<b>59.85</b>	87.46	79.41	75.63	46.91	39.11	36.43	76.09	61.04	53.73
CenterPoint (Ada3D-C)	<b>9.83×</b>	<b>8.49×</b>	<b>57.72</b>	82.52	74.98	69.11	43.66	38.23	34.80	75.27	59.96	52.14

Table 2: **Performance comparison of Ada3D on Nuscenes *val* set.** The “SPSS-Conv” model applies pruning for the 3D sparse convolution only, and the “CenterPoint-Mini” uses the 2D backbone with half the usual width.

Method	<i>FLOPs</i> <i>Opt.</i>	<i>Mem.</i> <i>Opt.</i>	mAP	NDS
PointPillar [8]	-	-	44.63	58.23
SECOND [21]	-	-	50.59	62.29
CenterPoint-Pillar [25]	-	-	50.03	60.70
CenterPoint [25] ( <i>voxel=0.1</i> )	-	-	55.43	64.63
CenterPoint-Ada3D ( <i>voxel=0.1</i> )	2.32×	2.61×	54.80	63.53
CenterPoint [25] ( <i>voxel=0.075</i> )	-	-	59.22	66.48
SPSS-Conv [11] ( <i>voxel=0.075</i> )	1.14×	1.14×	57.80	65.69
CenterPoint-Mini [25] ( <i>voxel=0.075</i> )	2.78×	2.78×	57.19	64.08
CenterPoint-Ada3D ( <i>voxel=0.075</i> )	3.34×	3.96×	58.62	65.68

with the drop rate  $R_{\text{drop}}$  to fit different resource budgets. “Ada3D-A” model only conducts adaptive inference for 2D backbone, it improves the model performance while reducing the dense rate of BEV features from 100% to 20% . “Ada3D-B” model reduces 40% 3D voxels and more than 80% 2D pixels and compresses the computaional and memory cost of the model by 5× without performance degradation. “Ada3D-C” model reduces 60% 3D voxels and more

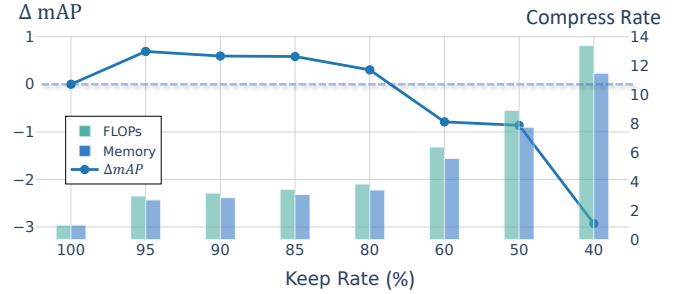


Figure 5: **Ada3D’s Performance under different  $R_{\text{drop}}$ .** Left: the relative mAP compared with baseline without Ada3D. Right: The FLOPs and memory compress rate.

than 90% 2D pixels with moderate performance loss, and reduces the model’s computation and memory cost by an order of magnitude. Table. 2 presents the performance on nuScenes, Ada3D optimized CenterPoint model achieves 2~4× FLOPs and memory savings with less than 1% performance drop. **Compared with methods that focus on reducing the model redundancy** (“CenterPoint-Mini” and “SPSS-Conv”), **Ada3D achieves a larger compression rate with less performance drop.**

### 4.3. Hardware Experiments

We conduct hardware profiling of the Ada3D model using sparse convolution GPU libraries [19, 2]. Fig.6 illustrates the reduction of GPU latency and peak memory for each layer, while Fig.7 presents the end-to-end hardware specs for the 3D and 2D backbones, respectively. From the results, we draw the following conclusions. First, by

Table 3: **Ablation studies and quantitive efficiency improvements of different Ada3D models on KITTI val.** “IP” stands for “importance predictor”, “DG” for “density-guided spatial filtering”, “SP-BN” for “sparsity preserving batch normalization”. The “FLOPs” and “Mem.” calculates the normalized resource consumption of the optimized model.

Method	Technique			FLOPs		Mem.		mAP (Mod.)	Car Mod. (IoU=0.7)	Ped. Mod. (IoU=0.5)	Cyc. Mod. (IoU=0.5)
	IP	DG	SP-BN	3D	2D	3D	2D				
CenterPoint	-	-	-	1.00	1.00	1.00	1.00	66.1	79.4 (-)	53.4 (-)	65.5 (-)
CenterPoint (SP-BN)	-	-	✓	1.00	0.49	1.00	0.45	66.0	79.1 (-0.3)	53.3 (-0.1)	65.6 (+0.1)
CenterPoint (Ada3D-A)	✓	✓	✓	1.00	0.22	1.00	0.25	66.4	79.5 (+0.1)	53.6 (+0.2)	66.1 (+0.6)
CenterPoint (Ada3D-B)	✓	✓	✓	0.66	0.18	0.68	0.17	66.1	79.1 (-0.3)	54.0 (+0.6)	65.3 (-0.3)
CenterPoint (Ada3D-B w.o. DG)	✓	-	✓	0.64	0.18	0.66	0.16	65.1	78.8 (-0.6)	51.6 (-1.8)	64.9 (-0.6)
CenterPoint (Ada3D-C)	✓	✓	✓	0.39	0.08	0.43	0.07	65.4	77.6 (-1.8)	53.5 (+0.2)	65.1 (-0.4)

using SP-BN and spatial filtering, we retain high sparsity of the 2D feature map, which brings significant reductions in peak memory and computation for the 2D backbone. For instance, the “conv2d\_1” layer shows a  $2.5\times$  latency and  $8.5\times$  memory improvement, and the overall memory of the 2D backbone is reduced by  $4.5\times$ ,  $6.7\times$ , and  $1.9\times$  for each model. Second, the end-to-end latency of the 3D backbone aligns with the drop rate. The latency for the 3D backbone is  $0.74\times$ ,  $0.56\times$ , and  $0.77\times$  of the pre-optimized ones, which corresponds to the drop rate (25%, 50%, 25%). Third, Ada3D is more effective for larger scenes and finer voxel sizes, since there exists more potential for exploiting the spatial sparsity. For the nuScenes Ada3D model, only peak memory optimization is achieved, but the latency remains similar. This is because that due to resource constraints, a larger voxel size is often used at the cost of inferior performance [20]. The nuScenes BEV feature map is processed in a relatively low resolution ([128, 128]), thus the dense rates of the deeper layer’s feature maps remain high, and using sparse convolution to process them takes longer than normal convolution. Future directions to improve this include further reducing redundancy or adopting more hardware acceleration techniques. Additionally, improving the efficiency could enable finer voxel size, which could in turn enhances performance and safety for safety-critic autonomous driving applicaiton.

## 5. Analysis and Discussions

### 5.1. Ablation Studies

**Importance predictor accurately evaluates the input features’ importance.** In Table. 3, comparing “Ada3D-A” and “SP-BN”, the predictor increases the 2D feature map’s sparsity from 50% to 80% upon SP-BN. As shown in Table. 4, Among the least important 25%/50% predicted, only 1.5%/7.8% features are mistakenly evaluated. Fig. 9 and Fig. 8 present the visualization of predictor heatmaps in both the BEV and voxel space. The predictor recognizes features within the box and avoids dropping them.

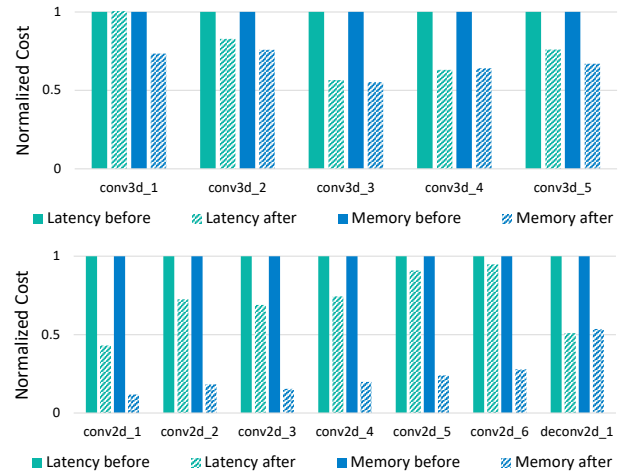


Figure 6: **Layer-wise GPU latency and peak memory optimization for Ada3D-B.** The green and blue bars stand for the latency and peak memory. The diagonal filled bars are Ada3D optimized costs.

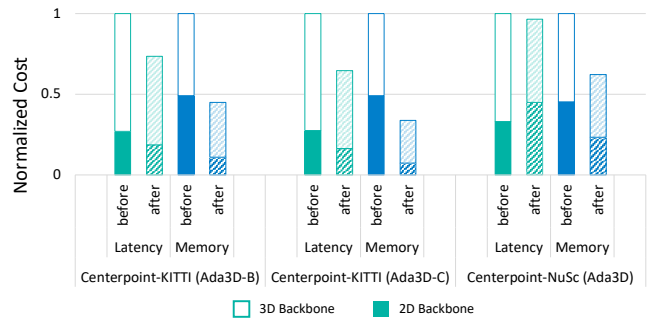


Figure 7: **End-to-end GPU latency and peak memory optimization for Ada3D.** The green and blue bars stand for the latency and peak memory cost respectively. The filled/unfilled bars represent the 2D/3D backbone.

**Density guidance avoids dropping the remote small-sized objects.** In Table. 3, comparing the “Ada3D-B” models with and without density guidance, simply using predictor scores causes notable performance degradation, especially for the pedestrian (-2.4%) with smaller sizes. Fig. 9 shows the example of density guidance correcting the drop of remote small objects. The predictor fails to correctly detect features for box-1,2,5 due to low density, and the density guidance compensates for such error. We also compare different importance criteria under different drop rates  $R_{drop}$  in Table. 4. The  $R_{inbox}$  denotes the percentage of dropped features that are in the ground-truth bounding box. Solely using the predictor score (IP) or density (DG) results in high  $R_{inbox}$  and performance degradation.

**SP-BN preserves the sparsity without performance drop.** Table. 3 shows that introducing the SP-BN increases the sparsity of 2D BEV features from 0% to 50% with no performance drop. In comparison, other BN schemes in Table. 5 cause performance or sparsity loss.

Table 4: **Comparison of adopting different importance criteria for input spatial filtering.** “IP” and “DG” stand for importance predictor and density guidance. The “ $R_{drop}$ ” represents the drop ratio. “ $R_{inbox}$ ” represents the percentage of dropped inputs that are within the ground truth bounding box (the lower the better).

$f_{score}$		$R_{drop}$	$R_{inbox}$		KITTI Mod. AP		
IP	DG		3D	2D	Car.	Ped.	Cyc.
-	-	-	-	-	79.1	53.3	65.6
-	✓	25%	12.3%	9.4%	76.4	45.6	59.4
✓	-	25%	1.4%	1.1%	78.8	51.6	64.9
✓	✓	25%	<b>0.8%</b>	<b>0.0%</b>	<b>79.1</b>	<b>54.0</b>	<b>65.2</b>
-	✓	50%	17.6%	20.3%	72.1	39.4	55.6
✓	-	50%	6.8%	8.8%	76.9	50.2	63.7
✓	✓	50%	<b>5.2%</b>	<b>7.5%</b>	<b>77.6</b>	<b>53.5</b>	<b>65.1</b>

Table 5: **Comparison of different BN types.** SP-BN maintains both performance and sparsity.

BN Type	Sparse	KITTI Mod. AP		
		Car.	Ped.	Cyc.
Normal BN	-	79.4	53.4	65.5
Without BN	✓	76.3	43.5	49.7
Nonzero BN	✓	65.7	33.4	42.1
SP-BN	✓	<b>79.1</b>	<b>53.3</b>	<b>65.6</b>

## 5.2. Analysis of the Adaptive Inference

**Ada3D introduces negligible overhead.** The extra cost that Ada3D introduces is the predictor inference. The pre-

dictor is conducted in a relatively low resolution and utilizes group convolution. The predictor’s computational cost is less than 1% of the 2D BEV backbone, which is negligible. The training cost of Ada3D includes a brief training of the predictor and model finetuning, which accounts for less than 30% of the original model’s training time.

**Ada3D could improve the performance** Adaptive inference removes redundant input features and saves computation and memory costs. However, adaptive inference does not necessarily have negative effects on performance. As shown in Table. 3 and Fig. 5, “Ada3D-A” improves the performance. We infer that the dropped redundant part is noisy and has negative effects on the training process.

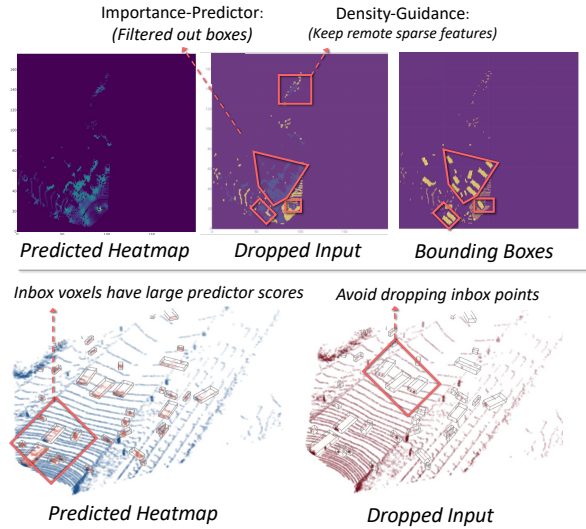


Figure 8: **Qualitative Results for 3D and 2D adaptive inference on KITTI and nuScenes dataset.** Visualization of the predicted heatmap and dropped input in BEV and voxel space. The predictor identifies the voxels/pixels inside the bounding box and avoids dropping them.

## 6. Conclusion

We propose Ada3D: an adaptive inference framework to reduce spatial redundancy for voxel-based 3D detectors. In order to identify and remove the redundant input, we design a shared lightweight predictor to evaluate the importance of input features. Spatial filtering is guided by the predictor score and density. SP-BN is introduced to maintain the sparsity of the 2D backbone. Extensive experiments demonstrate the superior performance and efficiency of the Ada3D optimized models.

## References

- [1] Michael Figurnov, Maxwell D Collins, Yukun Zhu, Li Zhang, Jonathan Huang, Dmitry Vetrov, and Ruslan



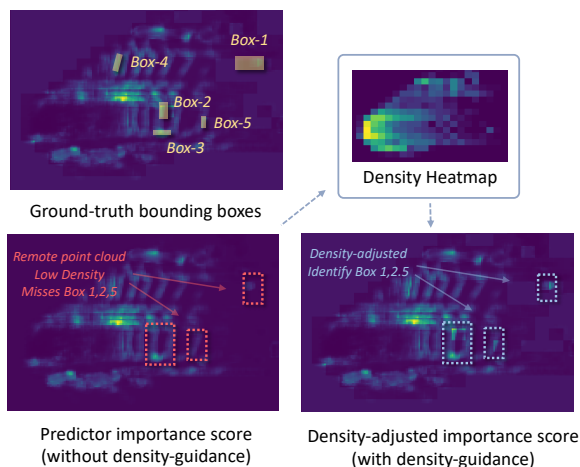


Figure 9: **Example of the density guidance corrects the drop of smaller remote objects.** Visualization of the predictor scores and density-guided scores.

Salakhutdinov. Spatially adaptive computation time for residual networks. In *Proceedings of the IEEE conference on computer vision and pattern recognition*, pages 1039–1048, 2017.

- [2] Benjamin Graham. Sparse 3d convolutional neural networks. In *British Machine Vision Conference*, 2015.
- [3] Sylvain Gugger. The 1cycle policy. <https://sgugger.github.io/the-1cycle-policy.html>, 2018.
- [4] Chen-Hang He, Huiyu Zeng, Jianqiang Huang, Xiansheng Hua, and Lei Zhang. Structure aware single-stage 3d object detection from point cloud. *2020 IEEE/CVF Conference on Computer Vision and Pattern Recognition (CVPR)*, pages 11870–11879, 2020.
- [5] Tiantian He, Haicang Zhou, Y. Ong, and Gao Cong. Not all neighbors are worth attending to: Graph selective attention networks for semi-supervised learning. *ArXiv*, abs/2210.07715, 2022.
- [6] Weizhe Hua, Christopher De Sa, Zhiru Zhang, and G. Edward Suh. Channel gating neural networks. In *Neural Information Processing Systems*, 2018.
- [7] Gao Huang, Yulin Wang, Kangchen Lv, Haojun Jiang, Wenhui Huang, Pengfei Qi, and Shiji Song. Glance and focus networks for dynamic visual recognition. *IEEE transactions on pattern analysis and machine intelligence*, PP, 2022.
- [8] Alex H. Lang, Sourabh Vora, Holger Caesar, Lubing Zhou, Jiong Yang, and Oscar Beijbom. Pointpillars: Fast encoders for object detection from point clouds. *2019 IEEE/CVF Conference on Computer Vision and Pattern Recognition (CVPR)*, pages 12689–12697, 2018.
- [9] Hongyang Li, Chonghao Sima, Jifeng Dai, Wenhui Wang, Lewei Lu, Huijie Wang, Enze Xie, Zhiqi Li, Hanming Deng, Haonan Tian, Xizhou Zhu, Li Chen, Yulu Gao, Xiangwei Geng, Jianqiang Zeng, Yang Li, Jiazhi Yang, Xiaosong Jia, Bo Yu, Y. Qiao, Dahua Lin, Siqian Liu, Junchi Yan, Jianping Shi, and Ping Luo. Delving into the devils of bird’s-eye-

view perception: A review, evaluation and recipe. *ArXiv*, abs/2209.05324, 2022.

- [10] Yujun Lin, Zhekai Zhang, Haotian Tang, Hanrui Wang, and Song Han. Pointacc: Efficient point cloud accelerator. *MICRO-54: 54th Annual IEEE/ACM International Symposium on Microarchitecture*, 2021.
- [11] Jianhui Liu, Yukang Chen, Xiaoqing Ye, Zhuotao Tian, Xiao Tan, and Xiaojuan Qi. Spatial pruned sparse convolution for efficient 3d object detection. *ArXiv*, abs/2209.14201, 2022.
- [12] Zhe Liu, Xin Zhao, Tengpeng Huang, Ruolan Hu, Yu Zhou, and Xiang Bai. Tanet: Robust 3d object detection from point clouds with triple attention. *ArXiv*, abs/1912.05163, 2019.
- [13] Oldpan. Pytorch-Memory-Utils: pytorch memory track code. <https://github.com/Oldpan/Pytorch-Memory-Utils>, May 4 2021. GitHub repository.
- [14] Mengye Ren, Andrei Pokrovsky, Bin Yang, and Raquel Urtasun. Sbnnet: Sparse blocks network for fast inference. In *Proceedings of the IEEE Conference on Computer Vision and Pattern Recognition*, pages 8711–8720, 2018.
- [15] Shaoshuai Shi, Chaoxu Guo, Li Jiang, Zhe Wang, Jianping Shi, Xiaogang Wang, and Hongsheng Li. Pv-rcnn: Point-voxel feature set abstraction for 3d object detection. In *Proceedings of the IEEE/CVF Conference on Computer Vision and Pattern Recognition*, pages 10529–10538, 2020.
- [16] Shaoshuai Shi, Xiaogang Wang, and Hongsheng Li. Point-rcnn: 3d object proposal generation and detection from point cloud. In *Proceedings of the IEEE/CVF conference on computer vision and pattern recognition*, pages 770–779, 2019.
- [17] Shaoshuai Shi, Zhe Wang, Jianping Shi, Xiaogang Wang, and Hongsheng Li. From points to parts: 3d object detection from point cloud with part-aware and part-aggregation network. *IEEE Transactions on Pattern Analysis and Machine Intelligence*, 43:2647–2664, 2019.
- [18] Vivienne Sze, Yu hsin Chen, Tien-Ju Yang, and Joel S. Emer. Efficient processing of deep neural networks: A tutorial and survey. *Proceedings of the IEEE*, 105:2295–2329, 2017.
- [19] Haotian Tang, Zhijian Liu, Xiuyu Li, Yujun Lin, and Song Han. Torchsparse: Efficient point cloud inference engine. *ArXiv*, abs/2204.10319, 2022.
- [20] Haotian Tang, Zhijian Liu, Shengyu Zhao, Yujun Lin, Ji Lin, Hanrui Wang, and Song Han. Searching efficient 3d architectures with sparse point-voxel convolution. In *Computer Vision–ECCV 2020: 16th European Conference, Glasgow, UK, August 23–28, 2020, Proceedings, Part XXVIII*, pages 685–702. Springer, 2020.
- [21] Yan Yan, Yuxing Mao, and Bo Li. Second: Sparsely embedded convolutional detection. *Sensors*, 18(10):3337, 2018.
- [22] Jinrong Yang, Lin Song, Songtao Liu, Zeming Li, Xiaoping Li, Hongbin Sun, Jian Sun, and Nanning Zheng. Dbq-ssd: Dynamic ball query for efficient 3d object detection. 2022.
- [23] Tianwei Yang. The centerpoint git repository. <https://github.com/tianweiy/CenterPoint-KITTI>, 2021.
- [24] Zetong Yang, Yanan Sun, Shu Liu, and Jiaya Jia. 3dssd: Point-based 3d single stage object detector. In *Proceedings of the IEEE/CVF conference on computer vision and pattern recognition*, pages 11040–11048, 2020.

- [25] Tianwei Yin, Xingyi Zhou, and Philipp Krahenbuhl. Center-based 3d object detection and tracking. In *Proceedings of the IEEE/CVF conference on computer vision and pattern recognition*, pages 11784–11793, 2021.
- [26] Linfeng Zhang, Runpei Dong, Hung-Shuo Tai, and Kaisheng Ma. Pointdistiller: structured knowledge distillation towards efficient and compact 3d detection. *CVPR*, 2022.
- [27] Xiangyu Zhang, Xinyu Zhou, Mengxiao Lin, and Jian Sun. Shufflenet: An extremely efficient convolutional neural network for mobile devices. *2018 IEEE/CVF Conference on Computer Vision and Pattern Recognition*, pages 6848–6856, 2017.
- [28] Yifan Zhang, Qingyong Hu, Guoquan Xu, Yanxin Ma, Jianwei Wan, and Yulan Guo. Not all points are equal: Learning highly efficient point-based detectors for 3d lidar point clouds. In *Proceedings of the IEEE/CVF Conference on Computer Vision and Pattern Recognition*, pages 18953–18962, 2022.
- [29] Tianchen Zhao, Niansong Zhang, Xuefei Ning, He Wang, Li Yi, and Yu Wang. Codedvtr: Codebook-based sparse voxel transformer with geometric guidance. *2022 IEEE/CVF Conference on Computer Vision and Pattern Recognition (CVPR)*, pages 1425–1434, 2022.
- [30] Yin Zhou and Oncel Tuzel. Voxelnet: End-to-end learning for point cloud based 3d object detection. In *Proceedings of the IEEE conference on computer vision and pattern recognition*, pages 4490–4499, 2018.